2017

A Novel Diffuse Fraction-Based Two-Leaf Light Use Efficiency Model: An Application Quantifying Photosynthetic Seasonality Across 20 AmeriFlux Flux Tower Sites

Hao Yan
University of Virginia, yanhaon@hotmail.com

Shao-Qiang Wang
Chinese Academy of Sciences

Kai-Liang Yu
University of Virginia

Bin Wang
University of Virginia

Qin Yu
The George Washington University

See next page for additional authors

Authors
Hao Yan, Shao-Qiang Wang, Kai-Liang Yu, Bin Wang, Qin Yu, Gil Bohrer, Dave P. Billesbach, Rosvel Bracho, and Faiz Rahman

AGU PUBLICATIONS

Journal of Advances in Modeling Earth Systems

RESEARCH ARTICLE
10.1002/2016MS000886

Key Points:
- A diffuse fraction based two leaf GPP model is developed
- Capture the unique seasonality in Amazon rainforest GPP, e.g., higher GPP in diffuse radiation-dominated wet season
- Diffuse radiation is more limiting than global radiation and water for Amazon rainforest GPP on a seasonal scale

Correspondence to:
H. Yan,
yanhaon@hotmail.com

Citation:
Yan, H., Wang, S.-Q., Yu, K.-L., Wang, B., Yu, Q., Bohrer, G., . . . Shugart, H. H. (2017). A novel diffuse fraction-based two-leaf light use efficiency model: An application quantifying photosynthetic seasonality across 20 AmeriFlux flux tower sites. *Journal of Advances in Modeling Earth Systems*, *9*, 2317–2332. https://doi.org/10.1002/2016MS000886

Received 8 DEC 2016
Accepted 14 SEP 2017
Accepted article online 20 SEP 2017
Published online 21 OCT 2017

A Novel Diffuse Fraction-Based Two-Leaf Light Use Efficiency Model: An Application Quantifying Photosynthetic Seasonality Across 20 AmeriFlux Flux Tower Sites

Hao Yan[1,2], Shao-Qiang Wang[3], Kai-Liang Yu[2], Bin Wang[2], Qin Yu[4], Gil Bohrer[5], Dave Billesbach[6], Rosvel Bracho[7], Faiz Rahman[8], and Herman H. Shugart[2]

[1]China Meteorological Administration, National Meteorological Center, Beijing, China, [2]Environmental Sciences Department, University of Virginia, Charlottesville, VA, USA, [3]Key Laboratory of Ecosystem Network Observation and Modeling, Institute of Geographic Sciences and Natural Resources Research, Chinese Academy of Sciences, Beijing, China, [4]Department of Geography, The George Washington University, Washington, DC, USA, [5]Department of Civil, Environmental and Geodetic Engineering, Ohio State University, Columbus, OH, USA, [6]Department of Biological Systems Engineering, University of Nebraska, Lincoln, NE, USA, [7]School of Forest Resources and Conservation, University of Florida, Gainesville, FL, USA, [8]Department of Geography, Indiana University, Bloomington, IN, USA

Abstract Diffuse radiation can increase canopy light use efficiency (LUE). This creates the need to differentiate the effects of direct and diffuse radiation when simulating terrestrial gross primary production (GPP). Here, we present a novel GPP model, the diffuse-fraction-based two-leaf model (DTEC), which includes the leaf response to direct and diffuse radiation, and treats maximum LUE for shaded leaves (ε_{msh} defined as a power function of the diffuse fraction (D_f)) and sunlit leaves (ε_{msu} defined as a constant) separately. An Amazonian rainforest site (KM67) was used to calibrate the model by simulating the linear relationship between monthly canopy LUE and D_f. This showed a positive response of forest GPP to atmospheric diffuse radiation, and suggested that diffuse radiation was more limiting than global radiation and water availability for Amazon rainforest GPP on a monthly scale. Further evaluation at 20 independent AmeriFlux sites showed that the DTEC model, when driven by monthly meteorological data and MODIS leaf area index (LAI) products, explained 70% of the variability observed in monthly flux tower GPP. This exceeded the 51% accounted for by the MODIS 17A2 big-leaf GPP product. The DTEC model's explicit accounting for the impacts of diffuse radiation and soil water stress along with its parameterization for C4 and C3 plants was responsible for this difference. The evaluation of DTEC at Amazon rainforest sites demonstrated its potential to capture the unique seasonality of higher GPP during the diffuse radiation-dominated wet season. Our results highlight the importance of diffuse radiation in seasonal GPP simulation.

Plain Language Summary As diffuse radiation can increase canopy light use efficiency (LUE), there is a need to differentiate the effects of direct and diffuse radiation in simulating terrestrial gross primary production (GPP). A novel diffuse-fraction (Df)-based two leaf GPP model (DTEC) developed by this study considers these effects. Evaluation at 20 independent flux tower sites using the MOD15 LAI product finds that the DTEC model explains 71% of the variability observed in monthly flux GPP. Evaluation at two Amazonian tropical forest sites (KM67 and KM83) indicates this model's potential to capture the unique seasonality in GPP, e.g., higher GPP in diffuse radiation-dominated wet season, while the two-leaf LUE GPP model (*He et al*., 2013) cannot due to using constant LUE for sunlit and shaded leaf. The DTEC model initially simulated the linear relationship between canopy LUE and D_f found at Amazon KM67 and KM83 forest sites. It shows a positive response of forest GPP to the atmosphere diffuse radiation in Amazon. Diffuse radiation was more limiting than global radiation and water for Amazon forest GPP on a seasonal scale. This differs from results of recent studies in which light-controlled leaf phenology plays the dominant role in seasonal variation of GPP in Amazonian.

1. Introduction

Plant photosynthesis utilizes atmospheric CO_2, water, and solar radiation to build tissues under the control of other environmental conditions such as temperature and nutrition (Monteith, 1972). Modeling of gross

Table 1
Big-Leaf and Two-Leaf GPP Models Regarding Impact of Diffuse Radiation

Model	Definition of impact of diffuse radiation and other stress factors[a]	Citation
CFLUX (Big leaf)	$GPP = \varepsilon \times FPAR \times PAR$ $\varepsilon = \varepsilon_{base} \times f(T_{min}) \times f(VPD) \times f(SM) \times f(S_a)$ $\varepsilon_{base} = (\varepsilon_{max} - \varepsilon_{cs}) * S_{CI} + \varepsilon_{cs}$ where ε is canopy light use efficiency (LUE), ε_{base} is base LUE, ε_{max} is maximum LUE, ε_{cs} is clear sky LUE, S_{CI} is cloudiness index (CI).	King et al. (2011)
CI-LUE (Big leaf)	$GPP = \varepsilon \times FPAR \times PAR$ $\varepsilon = \varepsilon_{base} \times f(T_a) \times f(VPD)$ $\varepsilon_{base} = (\varepsilon_{max} - \varepsilon_{cs}) * S_{CI} + \varepsilon_{cs}$	Wang et al. (2015)
DIFFUSE (Big leaf)	$GPP = \varepsilon \times FPAR \times PAR$ $\varepsilon = 0.024 \times D_f + 0.00061 \times \varepsilon_{max}$ where ε_{max} is maximum rate of photosynthesis with a value of 12 (μmol CO_2 m^{-2} s^{-1}) for tree, 20 for C3 grass, and 27 for C4 grass.	Donohue et al. (2014)
TL-LUE (Two leaf)	$GPP = (\varepsilon_{msu} \times APAR_{sun} + \varepsilon_{msh} \times APAR_{shd}) \times f(VPD) \times f(T_a)$ $APAR_{shd} = (1-\alpha) \times \left[\frac{PAR_{dif} - PAR_{dif,u}}{LAI} + C \right] \times LAI_{shd}$ where α is albedo; ε_{msu} and ε_{msh} are constant maximum LUE for sunlit and shaded leaves, and vary with site or biome type, e.g., evergreen broadleaf forest has ε_{msu}=0.73 (g C MJ^{-1}) and ε_{msh}=1.92 (g C MJ^{-1}).	He et al. (2013); Zhou et al. (2016)
DTEC (Two leaf)	$GPP = (\varepsilon_{msu} \times APAR_{sun} + \varepsilon_{msh} \times APAR_{shd}) \times f(E/E_{PT}) \times f(T_a)$ $APAR_{shd} = \left[\frac{PAR_{dif} - PAR_{dif,u}}{LAI} + C \right] \times LAI_{shd}$ $\varepsilon_{msh} = 3.78 \times D_f^{1.8}$ and $\varepsilon_{msu} = 1.67$ (g C MJ^{-1}) for C3 $\varepsilon_{msh} = 5.8 \times D_f^{1.8}$ and $\varepsilon_{msu} = 2.57$ (g C MJ^{-1}) for C4 where D_f is diffuse faction, E is actual evapotranspiration estimated from ARTS E model (Yan et al., 2012), E_{PT} is Priestley and Taylor (1972) potential evaporation.	This study

[a]Stress variables include temperature (T_{min} and T_a), water vapor pressure deficit (VPD), soil moisture (SM), standing age (S_a).

primary production (GPP) is central in connecting the global carbon, energy, and water cycles throughout the biosphere, atmosphere, hydrosphere, and pedosphere (Cramer et al., 2001). Because CO_2 is the primary greenhouse gas emitted through human activities (Cox et al., 2000), interest in GPP modeling is heightened by concerns associated with the sharply rising atmospheric CO_2 concentrations since the Industrial Revolution (Houghton, 2000; Nemani et al., 2003). Large variability still exists in our current GPP estimates of terrestrial ecosystems, especially on the global scale. This variability arises from uncertainties in canopy composition and structural complexity, environmental factors, and complexity of the underlying mechanisms of their interactions (Coops et al., 2009; Cramer et al., 1999; Wang et al., 2016; Xia et al., 2015).

Monteith (1972) pioneered the development of light-use-efficiency (LUE) theory, which states that photosynthetic production should correlate with the absorbed photosynthetically active radiation (APAR),

$$GPP = \varepsilon \times APAR = \varepsilon_{max} \times S_{stress} \times FPAR \times PAR \quad (1)$$

where GPP is the gross primary production (g C m^{-2}), ε is the actual LUE (g C MJ^{-1}) and is modified by environmental factors as $\varepsilon_{max} \times S_{stress}$, ε_{max} is the maximum LUE and S_{stress} refers to environmental stresses such as temperature and water stress. FPAR is the fraction of PAR absorbed by the canopy and PAR is the incident photosynthetically active radiation (MJ m^{-2}). Usually, the fraction of PAR contained in the incident global radiation R_g (MJ m^{-2}) is assumed to be 0.48 (McCree, 1972).

Different parameterizations of ε_{max} and S_{stress} have been proposed and applied, based on field experiments or calibrations against flux tower observations (Horn & Schulz, 2011; Maisongrande et al., 1995; Running et al., 2000; Yan et al., 2015). For example, the widely used MODIS GPP algorithm (Running et al., 2004) uses a biome-specific ε_{max} with a water stress factor defined as a function of vapor pressure deficit (VPD). Since C4 species have higher photosynthetic rates than C3 species (Baldocchi, 1994; Jones, 1992; Prince & Goward, 1995; Verma et al., 2005), the recent TEC GPP model (Yan et al., 2015) applied a universal ε_{max} of 1.8 g C MJ^{-1} for C3 species (Waring et al., 1995) and 2.76 g C MJ^{-1} for C4 species, respectively. The TEC model incorporates a water stress factor, defined as the ratio of actual evapotranspiration (Yan et al., 2012) to Priestley and Taylor (1972) potential evaporation (E_{PT}), for the effects of soil water availability and VPD.

Using remote sensing-derived FPAR data on regional and global scales, FPAR-based LUE models have been developed. Current LUE models based on Monteith (1972) theory, such as CASA (Potter et al., 1993), GLO-PEM (Prince & Goward, 1995), MOD17 (Running et al., 2000), VPM (Xiao et al., 2004), TOPS (Nemani et al., 2009), and TEC (Yan et al., 2015), often assume that GPP or NPP are linearly correlated with PAR. This implies that plant canopies act like one big leaf and the canopy absorbs direct and diffuse radiation at the same LUE during photosynthesis. The assumption is contradicted, however, by observations that canopy LUE strongly correlates with the diffuse-light fraction (D_f) (Choudhury, 2000; Farquhar & Roderick, 2003; Kanniah et al., 2013) and that diffuse radiation produces a higher LUE than direct radiation (Cheng et al., 2015, 2016). This LUE-D_f relationship is probably explained by the fact that shaded leaves are not light saturated while sunlit leaves can be (de Pury & Farquhar,1997; Gu et al., 2002; Knohl & Baldocchi, 2008). To include the impact of diffuse radiation, D_f has been incorporated to correct "big leaf" GPP models; for example, in the CFLUX model (King et al., 2011; Turner et al., 2006), the CI-LUE model (Wang et al., 2015), and the DIFFUSE model (Donohue et al., 2014) (Table 1).

The impact of diffuse radiation also depends on vegetation structure (Cheng et al., 2015). Shaded leaves in middle canopy layers often have a strong increase in leaf photosynthesis with diffuse radiation when compared to shaded leaves in the upper and lower canopy (Chen et al., 2012; Choudhury, 2000; Gu et al., 2002; Knohl & Baldocchi, 2008). This canopy-structure effect has not been considered in D_f-corrected big-leaf GPP models (Chen et al., 2012). Multilayer photosynthesis models have been successfully developed but they must be solved using numerical integration of photosynthesis from each layer of leaves. This complexity is numerically demanding but within the reach of modern digital computers (de Pury & Farquhar,1997; Sellers et al., 1992).

A simple and accurate alternative would conceptualize the canopy as being composed of sunlit and shaded leaves (Chen et al., 1999; de Pury & Farquhar, 1997; Norman, 1982). Accordingly, a two-leaf LUE model, TL-LUE (He et al., 2013; Table 1) was developed to include the impact of diffuse radiation. The TL-LUE model required a biome-dependent ε_{max} and ignored the effects of soil water. It uses temperature-stress and VPD-based water stress parameterizations that are derived from the MOD17 GPP algorithm. Despite these simplifications, the TL-LUE model generally performed better than the MOD17 GPP algorithm when tested at six flux sites in China (He et al., 2013) and at 98 FluxNet sites across the world (Zhou et al., 2016).

Table 2
Site Name, Abbreviation, Latitude (lat), Longitude (long), Country, Climate, Biome Type, and Years of Data of 21 AmeriFlux Sites

Site name	Abbreviation	Lat/Long	Country	Climate	Biome[a]	Years
LBA Tapajos KM67 Mature Forest	KM67	−2.85/−54.96	Brazil	Tropical	EBF	2002–2004
LBA Tapajos KM83 Logged Forest	KM83	−3.02/−54.97	Brazil	Tropical	EBF	2001–2003
Bartlett Experimental Forest	Bartlett	44.06/−71.29	USA	Temperate	DBF	2004–2005
UCI-1981 burn site	UCI1981	46.74/−91.17	Canada	Boreal	ENF	2002–2005
Univ. of Michigan Biological Station	UMBS	45.56/−84.71	USA	Temperate	DBF	2001–2003
Morgan Monroe State Forest	Morgan	39.32/−86.41	USA	Temperate	DBF	2001–2003
Metolius New Young Pine	MetoliusN	44.32/−121.61	USA	Temperate	ENF	2004–2005
Metolius Intermediate Pine	MetoliusI	44.50/−121.62	USA	Temperate	ENF	2005–2007
Mize	Mize	29.76/−82.24	USA	Subtropical	ENF	2001–2004
Wind River Crane Site	WindR	45.82/−121.95	USA	Mediterranean	ENF	2001–2002
Slashpine Donaldson	Donaldson	29.75/−82.16	USA	Subtropical	ENF	2001–2004
Vaira Ranch	Vaira	38.41/−120.95	USA	Mediterranean	Savanna	2001–2005
Tonzi Ranch	Tonzi	38.43/−120.97	USA	Mediterranean	Savanna	2002–2005
Santa Rita Mesquite Savanna	Santa	31.82/−110.87	USA	Subtropical	Shrub	2004–2006
Fermi Prairie	FermiP	41.84/−88.24	USA		Grass	2005–2006
Fermi Agricultural	FermiA	41.86/−88.22	USA		Crop	2005–2007
Bondville	Bondville	40.01/−88.29	USA	Temperate	Crop	2001–2004
ARM SGP Main	SGP	36.61/−97.49	USA	Temperate	Crop	2003–2005
Mead Rainfed	MeadR	41.17/−96.43	USA	Temperate	Crop	2002–2005
Mead Irrigated Rotation	MeadIR	41.16/−96.47	USA	Temperate	Crop	2002–2005
Mead Irrigated	MeadI	41.16/−96.47	USA	Temperate	Crop	2002–2005

[a]Evergreen broadleaf forest (EBF), Deciduous broadleaf forest (DBF), Evergreen needleleaf forest (ENF).

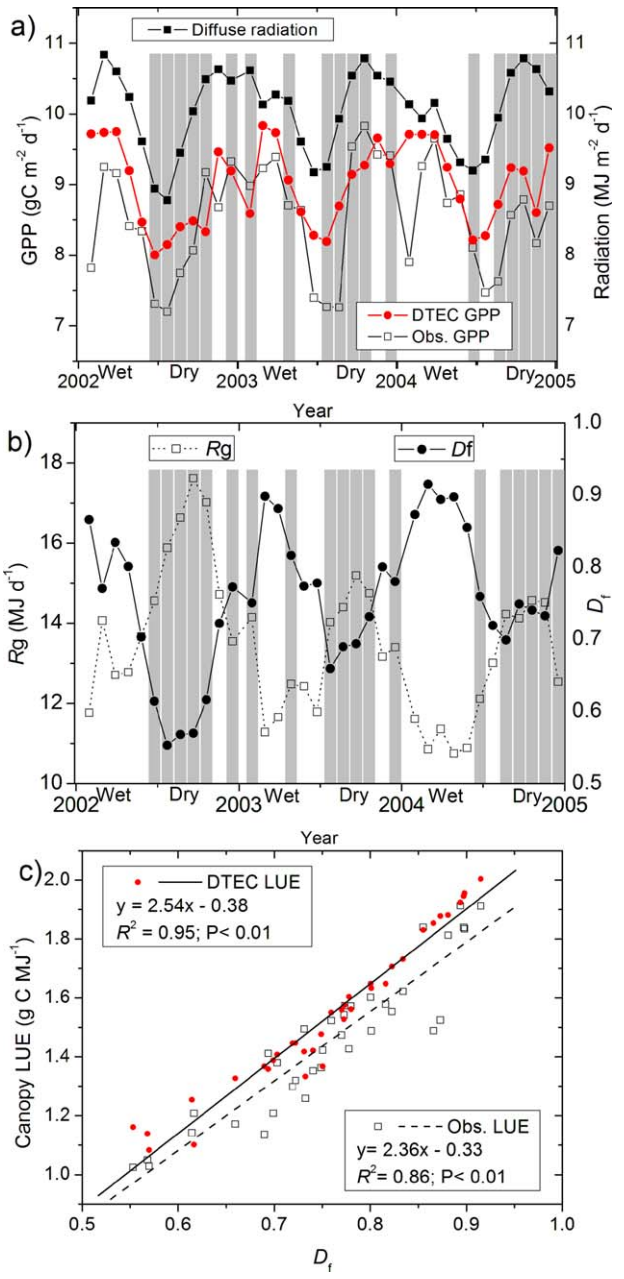

Figure 1. (a) Monthly flux tower-observed GPP, calibrated DTEC GPP, and calculated diffuse radiation over wet season and dry season (Grey color shows dry season defined as monthly precipitation $<$ 100 mm, (b) precipitation and global radiation R_g, and estimated diffuse fraction D_f), and (c) scatterplots of observed LUE and calibrated DTEC LUE versus D_f at the KM67 tropical Amazon forest site from 2002 to 2004.

Amazonian tropical evergreen forests have attracted much attention because of their dry/wet seasonality and corresponding small-amplitude seasonal cycle of photosynthesis, which was not successfully reproduced by some global biogeophysical models (Baker et al., 2008; Guan et al., 2015; Kim et al., 2012; Verbeeck et al., 2011; Wu et al., 2016). Similarly, few remote-sensing GPP models correctly simulated photosynthetic seasonality in the Amazon tropical forest. Previous studies have attributed the GPP seasonality in the Amazon forest to light-controlled leaf phenology (Kim et al., 2012), aggregate canopy phenology (Wu et al., 2016), or water availability (Guan et al., 2015). Our study explores the alternative hypothesis that diffuse radiation affects the GPP periodicity in the Amazon tropical forest.

We present here, a novel diffuse fraction (D_f)-based two leaf GPP model (DTEC), which incorporates and improves on the merits of the TL-LUE model and the TEC GPP model. The DTEC model allows consideration of the impacts of diffuse radiation as well as soil water. It requires monthly scale-inputs of LAI (obtained from MODIS), air temperature and relative humidity, incident global radiation, precipitation, and net radiation as drivers. The sections below present: (1) development of the DTEC GPP model and its calibration at an Amazon tropical forest site on a monthly scale, (2) evaluation of the DTEC model and MOD17 GPP product on monthly scales at 20 independent flux tower sites featuring a variety of biome types; (3) comparison of DTEC GPP and TL-LUE GPP at two Amazon forest sites; and (4) discussion and potential applications of the DTEC GPP model on a large scale.

2. Data Sets and Preprocessing

Monthly eddy covariance flux data, soil data, MODIS 8 day MOD15A2 LAI/FPAR and MOD17A2 GPP products were downloaded from Oak Ridge National Laboratory Distributed Active Archive Center (ORNL DAAC) (http://ameriflux.lbl.gov/) for use in this study. Monthly mean MODIS LAI/FPAR and GPP products were calculated using the 8 day MOD15A2 LAI/FPAR and MOD17A2 GPP after quality control so that MOD15A2 LAI data could be used to drive the DTEC GPP model coupled with monthly meteorological data, and so that MOD17A2 GPP data could be used to evaluate DTEC GPP model performance.

The DTEC GPP model was driven by monthly flux tower meteorological data as well as LAI data. It was calibrated against eddy covariance-derived GPP at an Amazon rainforest site (KM67), and then tested against observed GPP at 20 independent flux tower sites.

2.1. Eddy Covariance Data

Because the eddy covariance (EC) method measures CO_2, water, and energy fluxes between terrestrial ecosystem and the atmosphere, EC observations have been used to evaluate LUE and process-based GPP models (Baldocchi et al., 2001). Flux tower data were supplied by the ORNL DAAC at half hourly, daily, 8 day, and monthly time scales. GPP and meteorological data measured at 21 flux-tower sites were used in this study for calibrating and validating the GPP model. Note that the EC method directly measures net ecosystem exchange (NEE) not GPP at flux tower sites. Ecosystem respiration was estimated by using a simple temperature-dependent model (Falge et al., 2001). GPP was calculated as the difference between measured daytime NEE and estimated daytime respiration (Falge et al., 2002). The GPP estimates therefore inherited all the uncertainties of the NEE measurement and of the model for daytime respiration.

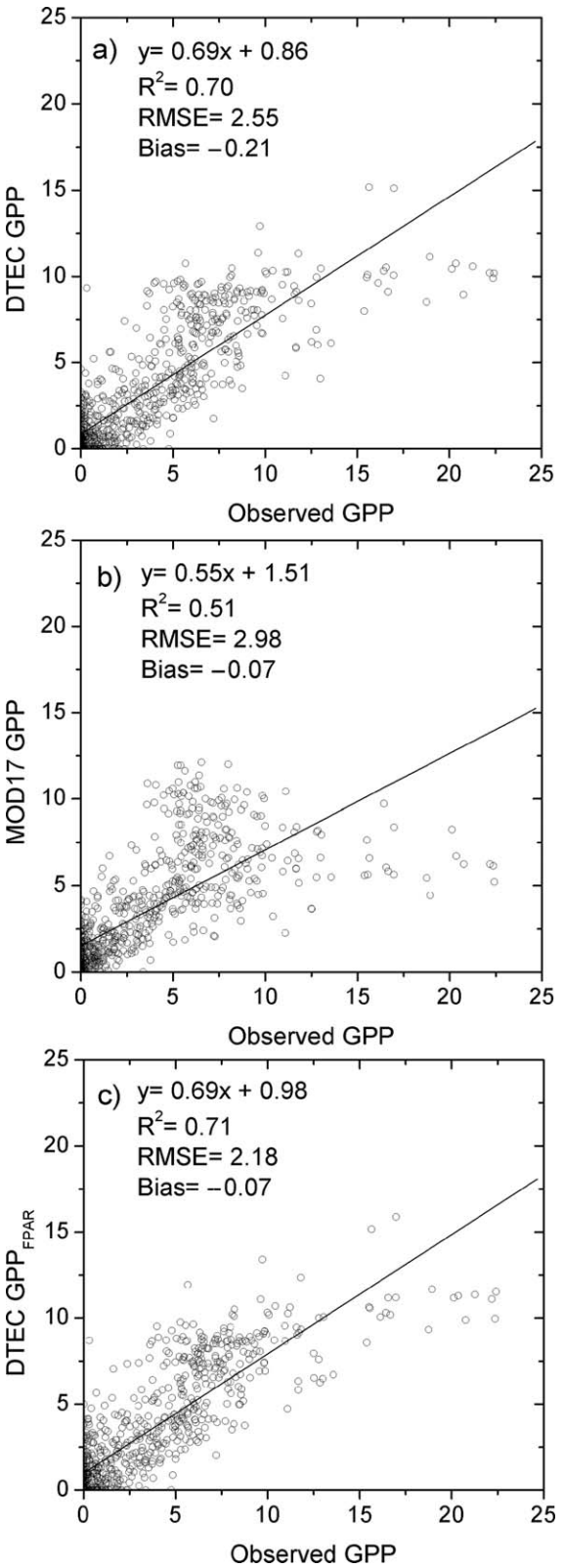

Figure 2. Scatterplot of observed GPP (g C m^{-2} d^{-1}) versus estimated (a) DTEC GPP driven with MOD15 LAI, (b) MOD17 GPP, and (c) DTEC GPP_{FPAR} driven with MOD15 FPAR-derived LAI for all data from 20 sites.

The KM67 site, an Amazon rainforest site, was adopted for calibration of the DTEC GPP model, while 20 independent sites were used for model evaluation. The 20 sites feature a wide range of ecosystem types including deciduous broadleaf forest, mixed forest, evergreen needleleaf forest, crop, grasslands, shrubland, savanna, and tropical forest (Table 2). Six sites (i.e., FermiP, FermiA, Bondville, MeadR, MeadIR, and MeadI) are mostly covered by C4 plants and the other 14 sites by C3 plants.

2.2. Soil Data

Soil data, including soil depth and soil texture (sand/silt/clay fractions), were downloaded from the ORNL DAAC and processed to calculate Maximum soil Available Water Content (MAWC) at 19 flux sites (Yan et al., 2012) using the parameterization proposed by Saxton et al. (1986).

Brazilian Amazon forests can access water in the soil to depths of 15 m (Nepstad et al., 1994) and tree roots can be found to a depth of 10 m according to field sampling (Bruno et al., 2006). This preserves sufficient soil water to maintain the high photosynthesis levels observed during the dry season (Hutyra et al., 2007). As a result, seasonal carbon dynamics (Baker et al., 2008) and the variation of soil water content at the KM67 site (Wu et al., 2016) were successfully simulated. By using a soil depth of 15 m (Nepstad et al., 1994) and setting the soil texture as clay (43% sand and 56% clay; Grant et al., 2009] at the tropical KM67 and KM83 sites, we derived a MAWC of ~2000 mm for driving the soil water balance model and estimating actual *E* using the ARTS *E* model (Yan et al., 2012). Note that observations, conducted in a tropical rainforest in French Guiana, show that some trees experience decreased photosynthesis when the relative extractable water decreases drastically (Stahl et al., 2013).

2.3. MOD15A2 LAI/FPAR Product

MODIS, as a satellite-borne instrument with 36 spectral bands covering wavelength from 0.4 μm to 14.4 μm, was designed for quantifying land, ocean, and atmosphere parameters on a global scale. It is the primary sensor onboard the National Aeronautics and Space Administration (NASA) sun-synchronous Terra satellite (10:30 AM local time descending node) and Aqua satellite (1:30 PM local time ascending node). To reduce the impact of clouds, an 8 day compositing procedure was applied to produce high quality, clear-sky land products. The MODIS LAI/FPAR products at 1 km spatial resolution were derived from up to 7 MODIS spectral bands using a three-dimension-radiative transfer model in a vegetative canopy (Myneni et al., 2002). A back-up LAI/FPAR algorithm, based on empirical MODIS specific NDVI-LAI and NDVI-FPAR relationships, was adopted when the main radiative transfer algorithm failed due to clouds or other atmospheric impacts (Yang et al., 2006).

MOD15A2 LAI/FPAR products were downloaded from ORNL DAAC in a form of ASCII data covering a 7 × 7 km^2 area centered on each flux tower site. With its companion quality control data, all poor quality LAI/FPAR data were checked and replaced by linear interpolation from the nearest reliable data (Zhao et al., 2005). For each site, LAI from the central pixel at the coordinate position of a flux tower were extracted for calculating GPP and *E* in the DTEC model.

2.4. MOD17A2 GPP Product

The MOD17A2 C51 8 day GPP/NPP products at 1 km spatial resolution were downloaded from the ORNL DAAC as ASCII subset data for comparison with GPP estimates from the DTEC model at 20 flux sites in this study. The MODIS GPP algorithm (Running et al., 2004) follows the Monteith (1972) LUE theory,

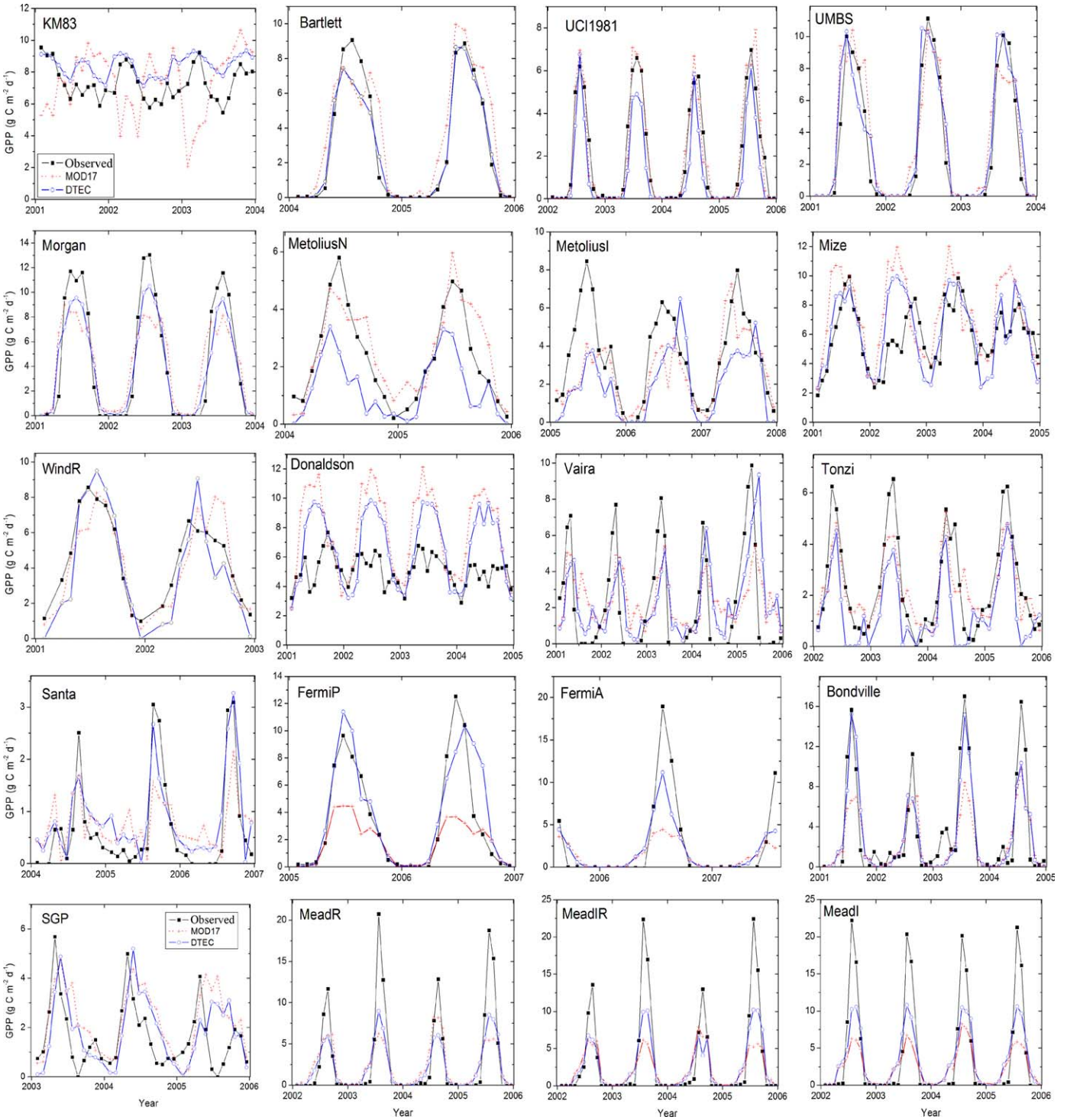

Figure 3. Comparison of monthly flux tower-observed GPP versus estimated MOD17 GPP and DTEC GPP at 20 flux sites.

$$\mathrm{GPP}=\varepsilon_{max}\times m(T_{min})\times m(\mathrm{VPD})\times \mathrm{FPAR}\times \mathrm{PAR} \quad (2)$$

where ε_{max} is the biome-specific maximum conversion efficiency, $m(T_{min})$ reduces ε_{max} as a scaler when the minimum air temperature (T_{min}) limits plant growth, VPD is vapor pressure deficit, and m(VPD) is another scaler used to reduce ε_{max} when VPD is high enough to inhibit photosynthesis, PAR is the incident photosynthetically active radiation, and FPAR is the fraction of PAR absorbed by the canopy.

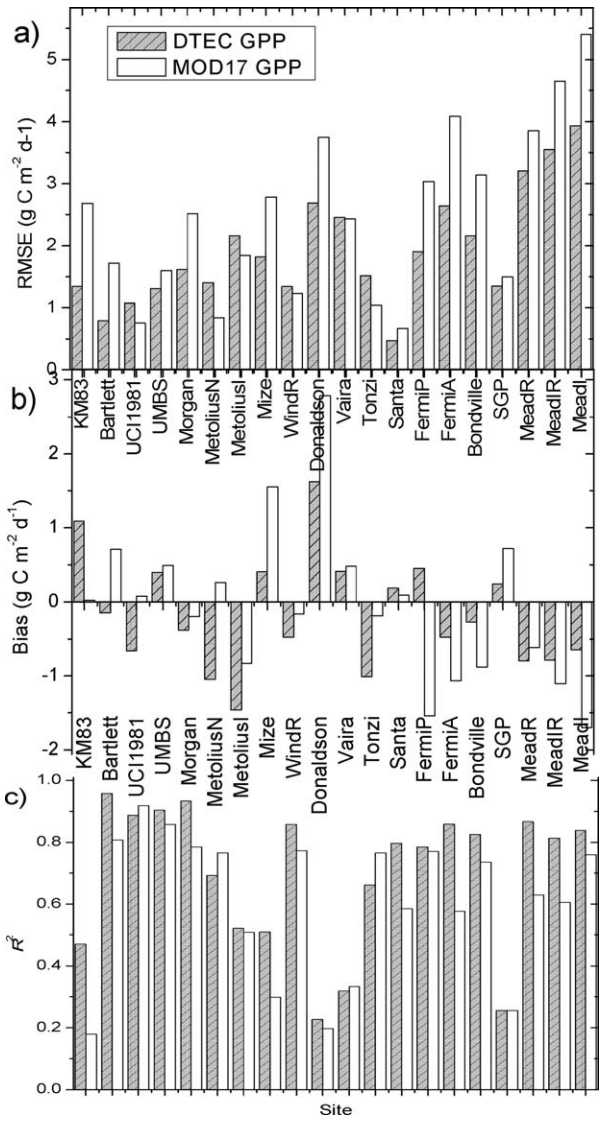

Figure 4. Monthly statistics of (a) RMSE, (b) Bias, and (c) R^2 for estimated DTEC GPP and MOD17A2 GPP versus observed GPP at 20 flux sites.

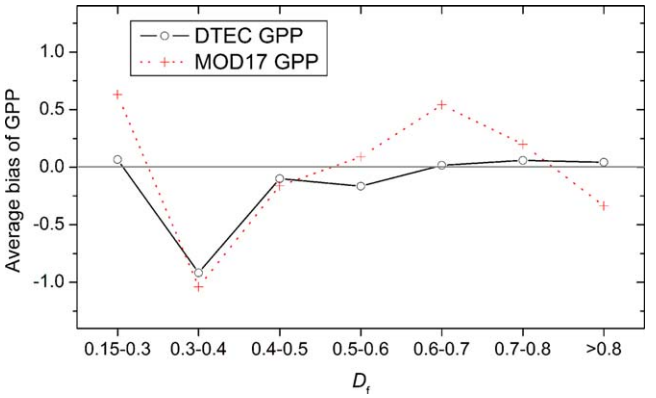

Figure 5. Bias of estimated DTEC and MOD17 GPP (g C m^{-2} d^{-1}) averaged over bins of diffuse fraction D_f for all data at 20 flux sites.

The standard MOD17A2 GPP/NPP global products were calculated from the Data Assimilation Office (DAO) meteorological reanalysis data, biome type-specific maximum conversion efficiency, and MOD15A2 FPAR product (Zhao et al., 2005). The MOD17 GPP products have been tested as a standard GPP product by several GPP-modeling studies (Donohue et al., 2014; He et al., 2013; Yan et al., 2015).

3. The Diffuse Fraction-Based Two-Leaf Terrestrial Ecosystem Carbon Flux Model (DTEC)

3.1. Development of the DTEC GPP Model

The DTEC GPP model was developed based on the two leaf-light use efficiency TL-LUE model that separates contributions of sunlit and shaded leaves (Chen et al., 1999; He et al., 2013), and the big leaf TEC LUE model (Yan et al., 2015) that explicitly considers the impact of water stress by using a precipitation-driven evapotranspiration model (Yan et al., 2012). The DTEC GPP model is defined as,

$$\mathrm{GPP}=(\varepsilon_{msu}\times\mathrm{APAR}_{sun}+\varepsilon_{msh}\times\mathrm{APAR}_{shd})\times W_\varepsilon\times T_\varepsilon \quad (3)$$

where ε_{msu} and ε_{msh} are maximum LUE (g C MJ^{-1}) for sunlit and shaded leaves, respectively, APAR_{sun} and APAR_{shd} are incident photosynthetically active radiation (PAR) absorbed by sunlit and shaded leaves, W_ε and T_ε are water and temperature stress factors, respectively.

APAR_{sun} and APAR_{shd} follow the definition given by Norman (1982), and also used by Chen et al. (1999) and He et al. (2013),

$$\mathrm{APAR}_{sun}=\left[\mathrm{PAR}_{dir}\times\frac{\cos(\beta)}{\cos(\theta)}+\frac{\mathrm{PAR}_{dif}-\mathrm{PAR}_{dif,u}}{\mathrm{LAI}}+C\right]\times\mathrm{LAI}_{sun} \quad (4)$$

$$\mathrm{APAR}_{shd}=\left[\frac{\mathrm{PAR}_{dif}-\mathrm{PAR}_{dif,u}}{\mathrm{LAI}}+C\right]\times\mathrm{LAI}_{shd} \quad (5)$$

$$\mathrm{LAI}_{sun}=2\times\cos(\theta)\times\left[1-\exp\left(-0.5\times\Omega\times\frac{\mathrm{LAI}}{\cos(\theta)}\right)\right] \quad (6)$$

$$\mathrm{LAI}_{shd}=\mathrm{LAI}-\mathrm{LAI}_{sun} \quad (7)$$

where PAR_{dif} and PAR_{dir} are diffuse and direct radiation (MJ m^{-2}) of PAR, respectively. $\mathrm{PAR}_{dif,u}$ is diffuse radiation under the canopy, C represents the contribution of multiple scattering of direct radiation to the diffuse radiation (Norman, 1982), β is the mean leaf-sun angle and is set to 60° for a canopy with spherical leaf angle distribution (Chen et al., 1999), θ is the solar zenith angle, Ω is the clumping index which is dependent on vegetation types and is set to 0.6, 0.8, 0.7, 0.9, 0.9, 0.5, and 0.7 for evergreen conifer forest, evergreen broadleaf forest, mixed forest, grass, crop, boreal conifer forest, and boreal deciduous forest, respectively (Chen et al., 1999; He et al., 2013). LAI_{sun} and LAI_{shd} are the leaf area index (LAI) of sunlit and shaded leaves, respectively.

Diffuse radiation PAR_{dif} is calculated from the sky clearness index (SI)-based diffuse faction (D_f) following the method of He et al. (2013),

$$\mathrm{PAR}_{dif}=\mathrm{PAR}\times D_f \quad (8)$$

$$D_f=0.7527+3.8453\mathrm{SI}-16.316\mathrm{SI}^2+18.962\mathrm{SI}^3-7.0802\mathrm{SI}^4 \quad (9)$$

$$\mathrm{SI}=\mathrm{PAR}/[0.48S_0\cos(\theta)] \quad (10)$$

where PAR is a fraction (0.48) of incident global radiation R_g (McCree, 1972), and S_0 is the solar constant (1367 W m^{-2}).

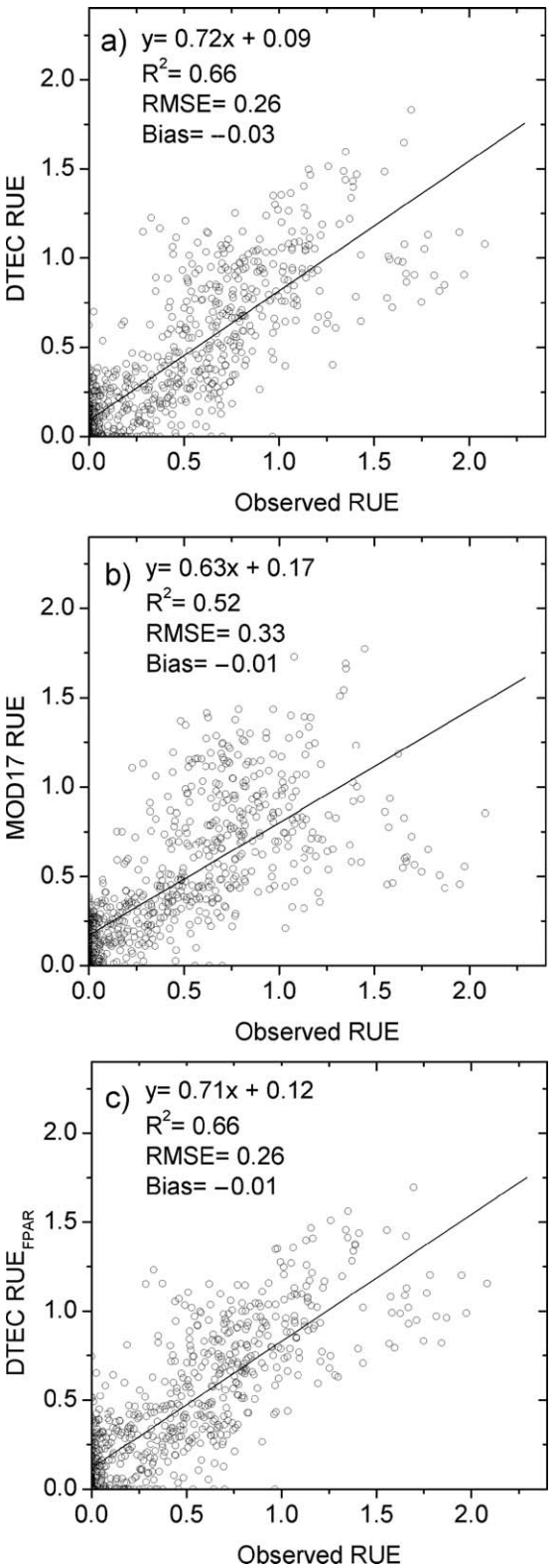

Figure 6. Scatterplot of observed radiation use efficiency (RUE = GPP/PAR) versus estimated (a) DTEC RUE (i.e., DTEC GPP/PAR), (b) MOD17 RUE (i.e., MOD17 GPP/PAR), and (c) DTEC RUE_{FPAR} (i.e., DTEC GPP_{FPAR}/PAR) for all data from 20 sites.

The water stress factor W_ε is calculated following the TEC-flux model (Yan et al., 2015),

$$W_\varepsilon = E/E_{PT} \tag{11}$$

where E_{PT} is the potential evaporation (Priestley & Taylor, 1972) and E is actual evapotranspiration calculated from the ARTS E Model (Yan et al., 2012). Assuming no water stress, the ARTS E model first calculates total E (E_0) as a sum of vegetation transpiration E_c and soil evaporation E_s. Then, a precipitation-driven soil water balance model is applied to scale E_0 to actual E. ARTS E has been applied to diagnostic analysis of interannual variation of global terrestrial evapotranspiration (Yan et al., 2013) and global drought monitoring from 1982 to 2011 (Yan et al., 2014).

The temperature-stress factor T_ε is calculated from the Terrestrial Ecosystem Model (TEM) (Raich et al., 1991),

$$T_\varepsilon = \frac{(T_a - T_{min})(T_a - T_{max})}{(T_a - T_{min})(T_a - T_{max}) - (T_a - T_{opt})^2} \tag{12}$$

where T_a is the air temperature (°C), T_{min}, T_{max}, and T_{opt} are biome-specific minimum, maximum, and optimum temperatures for photosynthetic activity, respectively (Melillo et al., 1993).

3.2. Calibration of the DTEC GPP Model

It is widely acknowledged that photosynthesis in sunlit leaves is often light-saturated producing a lower LUE. In contrast, photosynthesis in shaded leaves is usually not light-saturated and thus has a higher LUE (Chen et al., 1999; de Pury & Farquhar, 1997; Zhang et al., 2012). Few studies however, address the relationship between canopy LUE and D_f, or apply these relationships in GPP simulation. Calibration experiments for the two-leaf TL-LUE model in several flux sites indicate that ε_{msh} is 2.5 to 4.6 times higher than ε_{msu} (He et al., 2013; Zhou et al., 2016).

Flux tower GPP data measured at the tropical Amazon site of KM67 in the Tapajos National Forest of Brazil from 2002 to 2004 was used to calibrate the DTEC GPP model for C3 plants. At the KM67 site, GPP varies seasonally with a peak of about 9.2 g C m^{-2} d^{-1} in the wet season and a lower value of about 7.4 g C m^{-2} d^{-1} in the dry season (Figure 1a). Conversely, observed global radiation (R_g) at the KM67 site (Figure 1b) has the opposite seasonal variation with a lower value of about 11.2 MJ m^{-2} d^{-1} in the wet season and a higher value of about 15.2 MJ m^{-2} d^{-1} in the dry season (monthly precipitation less than 100 mm). The KM67 site-derived-diffuse radiation, however, varies as GPP indicating a significant contribution of the diffuse-light component to GPP (Figure 1a). The observed LUE shows a significant linear relation to D_f, which highlights D_f 's potential in estimating LUE as well as GPP (Figure 1c).

Observed LUE was calculated from monthly observed GPP, global radiation R_g, and camera-derived FPAR according to the Penman LUE theory,

$$\mathrm{LUE} = \mathrm{GPP}/(\mathrm{PAR} \times \mathrm{FPAR}) = \mathrm{GPP}/\left(0.48 \times R_g \times \mathrm{FPAR}\right) \tag{13}$$

As sunlit leaves receive direct and diffuse radiation while shaded leaves only receive diffuse radiation (Mercado et al., 2009), it is assumed in this study that ε_{msu} for sunlit leaves is a constant. Since the ε_{msh} of shaded leaves changes with D_f, it is assumed to be a power function of D_f. The observed monthly LAI and FPAR at KM67 by Wu et al. (2016), coupled with meteorological data measured by the flux tower, were used to calibrate the DTEC GPP model and to derive the unknown parameters of ε_{msu} and ε_{msh}.

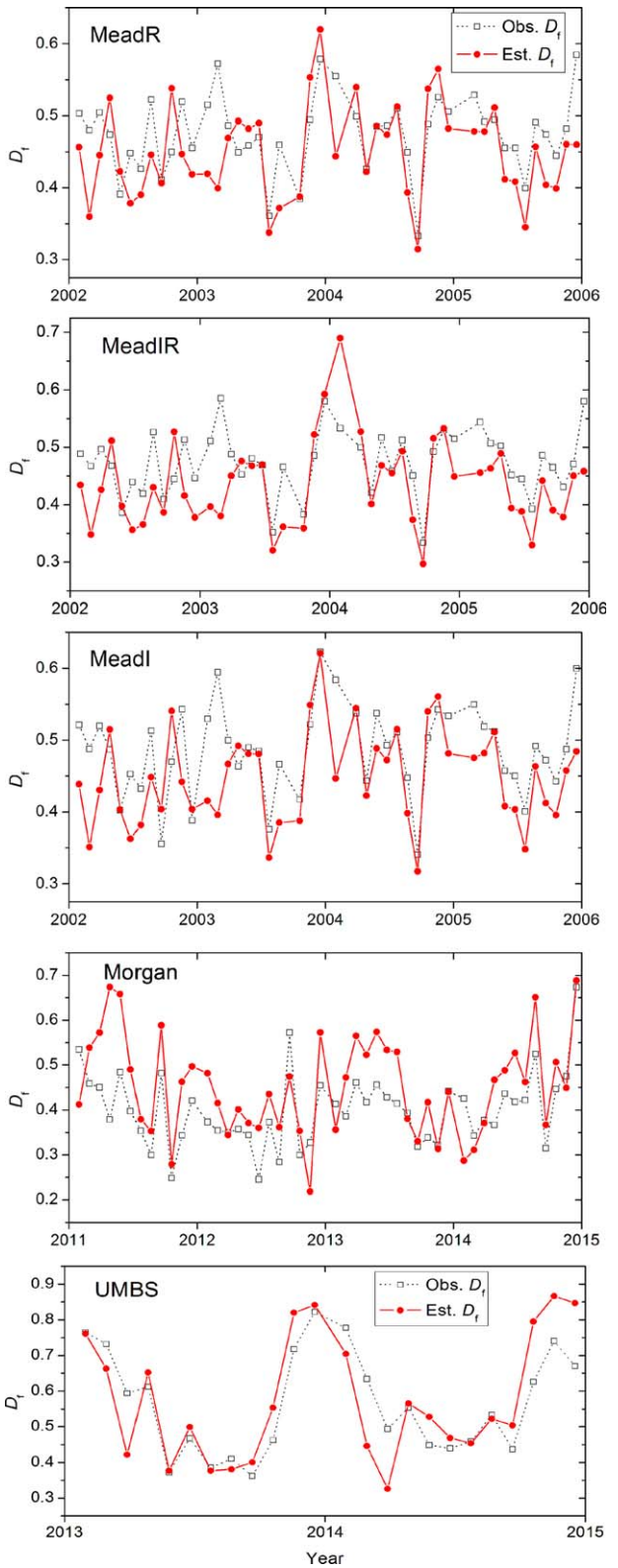

Figure 7. Monthly variations of the observed D_f and estimated D_f at five sites, MeadR, MeadIR, MeadI, Morgan, and UMBS.

ε_{msu} and ε_{msh} were estimated by a procedure where the root mean square error (RMSE) of DTEC LUE versus the observed LUE was minimized and where the calibrated DTEC GPP preserved a seasonal variation, similar to the flux tower-observed GPP (Figure 1a). For C3 plant,

$$\varepsilon_{msh} = 3.78 \times D_f^{1.8} \text{ and } \varepsilon_{msu} = 1.67 \quad (14)$$

where D_f is the diffuse fraction. In the big leaf-based TEC GPP model (Yan et al., 2015), C4 plants have an ε_{max} value of 2.76 (Prince & Goward, 1995) which is about 1.53 times higher than for C3 plants. We therefore used this same ratio to derive C4 values for ε_{msu} and ε_{msh} for the DTEC model.

$$\varepsilon_{msh} = 5.78 \times D_f^{1.8} \text{ and } \varepsilon_{msu} = 2.56 \quad (15)$$

4. Results

4.1. Evaluation of the DTEC GPP Model

After calibration at the KM67 site, flux tower-observed GPP data from 20 AmeriFlux sites (Table 2) were used to evaluate the DTEC GPP model at a monthly scale. In these tests, DTEC's GPP predictions showed better performance against the flux tower observed GPP than MOD17A2 GPP. The DTEC model simulated monthly GPP for all sites with overall statistics of $R^2 = 0.70$, RMSE = 2.55 g C m^{-2} d^{-1}, and bias = −0.21 g C m^{-2} d^{-1} (Figure 2a). The MOD17 GPP predicted monthly GPP with overall statistics of $R^2 = 0.51$, RMSE = 2.98 g C m^{-2} d^{-1}, and bias = −0.07 g C m^{-2} d^{-1} for all sites (Figure 2b).

Figure 3 shows the seasonal dynamics of monthly estimated DTEC GPP and MOD17 GPP versus flux tower-observed GPP at the 20 flux sites, respectively. For the KM83 Amazon rainforest site, MOD17 GPP produced a relatively large error for the seasonal variation due to a higher value than the observed GPP in the dry season and a lower value than observed GPP during the wet season while the DTEC GPP captured the seasonal dynamics of GPP more accurately. MOD17 GPP significantly underestimated GPP at all C4 sites including FermiP, FermiA, Bondville, SGP, MeadR, MeadIR, and MeadI, while DTEC GPP provided improved GPP estimates at all C4 sites compared with MOD17 GPP estimates. This supports the effectiveness of different parameterizations for C3 and C4 plants in the DTEC model. At the other 12 C3 sites, both DTEC GPP and MOD17 GPP captured the seasonal dynamics of GPP.

Compared to observations, the DTEC GPP often had a lower RMSE, a lower absolute value of bias, and a higher R^2 than the MOD17 GPP (Figure 4). This was especially obvious at the Amazon KM83 site and at all sites dominated by C4 plants. The DTEC GPP had an average RMSE of 1.93 g C m^{-2} d^{-1} varying from 0.47 g C m^{-2} d^{-1} at Santa to 3.93 g C m^{-2} d^{-1} at MeadI, while the MOD17A2 GPP had a mean RMSE of 2.47 g C m^{-2} d^{-1} varying from 0.67 g C m^{-2} d^{-1} at Santa to 5.40 g C m^{-2} d^{-1} at MeadI (Figure 4a). Similarly, the DTEC GPP had an average R^2 of 0.7 with a range from 0.23 at Donaldson to 0.96 at Barlett while the MOD17A2 GPP had a lower mean R^2 of 0.6 with a range from 0.01 at KM67 to 0.92 at UCI1981 (Figure 4c).

The performance statistics of DTEC was similar to other D_f-corrected big leaf LUE models. For example, the DIFFUSE GPP model (driven with MOD15 FPAR data and specific ε_{max} for tree, C3 grass, and C4 grass) gave a monthly based $R^2 = 0.75$ at 12 flux tower sites across Australia (Donohue et al., 2014). The CFLUX GPP model, driven with MOD15 FPAR data and site-calibrated ε_{max} and clear sky LUE (ε_{cs}), was validated at 18 flux tower sites across North America

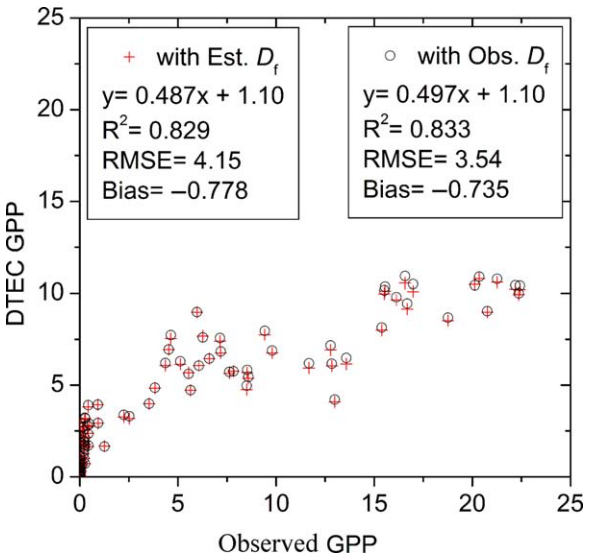

Figure 8. Scatterplot of observed GPP (g C m^{-2} d^{-1}) versus estimated DTEC GPP driven with observed D_f and estimated D_f of He et al. (2013) at monthly scales for all data from MeadR, MeadIR, and MeadI sites.

producing an RMSE ranging from 0.91g C m^{-2} d^{-1} at temperate grass sites to 3.44 g C m^{-2} d^{-1} at temperate crop sites (King et al., 2011). As a two-leaf remote sensing model, the TL-LUE model, driven with MODIS LAI data and site-calibrated ε_{msu} and ε_{msh}, had an RMSE of 0.60 to 2.17 g C m^{-2} d^{-1} and R^2 of 0.48 to 0.93 for six sites in China (He et al., 2013). Further validation of TL-LUE GPP at 98 FLUXNET sites distributed across the globe, driven with biome-specific ε_{msu} and ε_{msh}, resulted in an RMSE of 0.54–3.54 g C m^{-2} d^{-1} and R^2 of 0.5 to 0.9 for nine biomes (Zhou et al., 2016). All of the above LUE models incorporate the effect of diffuse radiation and show error statistics better than that of MOD17 GPP products.

We calculated the bias of GPP estimates from DTEC and MOD17, averaged over bins of diffuse fraction for all 20 flux sites. Figure 5 shows that DTEC GPP had a very small bias when D_f was above 0.4 while MOD17 GPP underestimated GPP for D_f higher than 0.8 and overestimated GPP for D_f between 0.6 and 0.7. Overall, the DTEC GPP model as a two leaf model had a superior performance to MOD17 GPP in high D_f environments. We note that both DTEC and MOD17 GPP underestimated GPP for D_f in the range of 0.3 to 0.4 (Figure 5), mainly due to underestimation of GPP for C4 crops (Figure 3). This partially arises from an underestimation of MODIS LAI for crops (Matsui et al., 2008; Yan et al., 2015) when compared with field-observed LAI at the MeadI, MeadIR, and MeadR flux sites (Verma et al., 2005). This suggests that an improved remote-sensing algorithm for C4 species is needed.

Because estimated GPP contains an input error from PAR data, observed and estimated radiation use efficiencies (RUE) were calculated such that the DTEC GPP model could be evaluated from an alternate approach for RUE computation where the impact of PAR was removed. RUE was defined as GPP divided by PAR (Choudhury, 2000). Figure 6 shows that the DTEC RUE estimates had statistics of RMSE= 0.26, Bias= −0.03, and R^2= 0.66 (Figure 6a) while MOD17 RUE yielded RMSE= 0.33, Bias= −0.01, and R^2= 0.52 (Figure 6b). The DTEC GPP model simulated the monthly RUE for all data from the 20 sites with better error statistics than that of MOD17 GPP products.

4.2. Evaluation of the Diffuse Fraction Model

Since D_f plays a key role in simulating GPP by the DTEC model, it is important to evaluate the estimation of D_f from PAR and clear-sky index, as done by the D_f model using equation (9) (He et al., 2013). Among 20 flux sites, only MeadR, MeadIR, MeadI, Morgan, and UMBS sites provide observation of D_f derived from observed diffuse radiation and global radiation. Figure 7 shows that estimated D_f from equation (9) could capture monthly variations of observed D_f at these five sites, which validates its potential for estimating diffuse radiation. DTEC GPP also was calculated by using observed D_f instead of estimated D_f (He et al., 2013) for all data at MeadR, MeadIR, and MeadI. Figure 8 shows that DTEC GPP driven with observed D_f and estimated D_f at monthly scales had similar error statistics relative to observed GPP.

We also evaluated the DTEC model's sensitivity to the different SI-based D_f equations developed by Chen et al. (1999) and Roderick et al. (2001), respectively.

$$D_f = 0.943 + 0.734SI - 4.9SI^2 + 1.796SI^3 + 2.058SI^4 \quad (16)$$

$$D_f = 1.11 - 1.31SI \quad (17)$$

Figure 9 shows that DTEC GPP_{chen} and $GPP_{Roderick}$ had similar error statistics of RMSE= 2.26 and R^2= 0.70, which were almost equivalent except for bias to the error of DTEC GPP (GPP_{He}; see Figure 2a) when driven with the He et al. (2013) D_f equation. DTEC GPP_{He} had a bias of −0.21 for all data (Figure 2a), while DTEC GPP_{chen} and $GPP_{Roderick}$ gave a larger underestimation of GPP with a bias of −0.37; even lower than that of DTEC GPP_{He}. Overall, the DTEC GPP model was sensitive to the choice of D_f estimation equation and different D_f equations might result in systematic biases of GPP estimations.

4.3. Improvements of DTEC GPP to TL-LUE GPP in Amazon Rainforests

The Amazon tropical region (e.g., the KM67 Amazon rainforest site, see Figure 1a) features high diffuse radiation and D_f, which supplies a testbed to evaluate the model performance in simulating the effect of diffuse

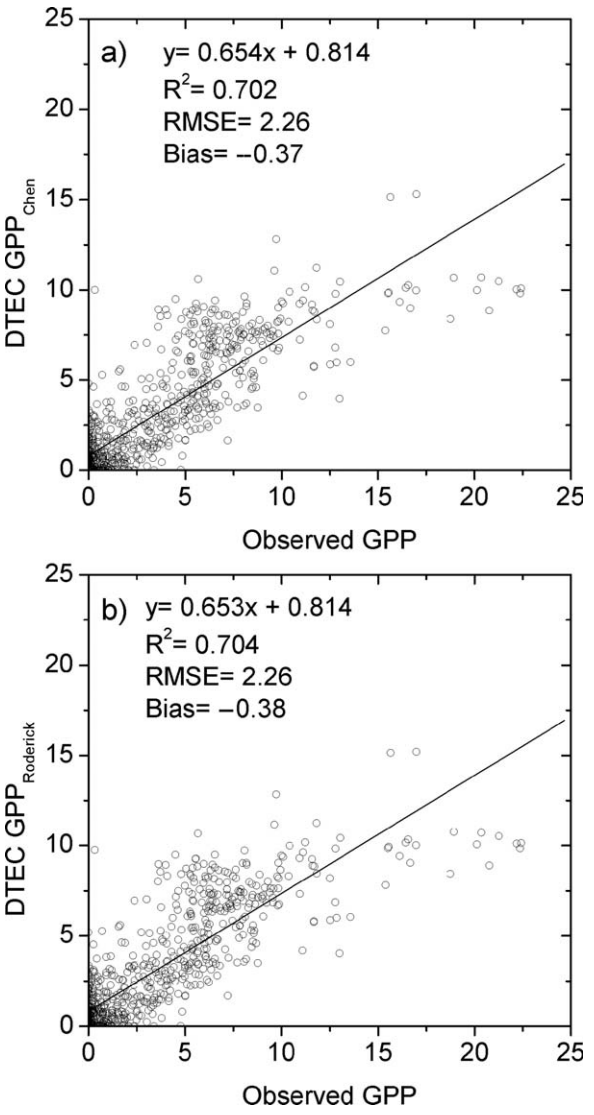

Figure 9. Scatterplot of monthly observed GPP (g C m^{-2} d^{-1}) versus estimated (a) DTEC GPP_{chen} and (b) DTEC $GPP_{Roderick}$ driven with D_f of Chen et al. (1999) and Roderick et al. (2001) respectively for all data from 20 sites.

radiation. Following the parameterization of the TL-LUE model for evergreen broadleaf forest with a constant of ε_{msu}=0.73 and ε_{msh}=1.92 (g C MJ^{-1}) for sunlit and shaded leaves respectively (Zhou et al., 2016), TL-LUE GPP was estimated at KM67 and KM83Amazon sites from MOD15A2 LAI and MCD43C3 Albedo products and flux tower data on monthly scales. Comparison with flux tower-observed GPP (Figure 10) shows that the TL-LUE GPP model simulated the GPP seasonality with poorer performance statistics at the KM67 site (Bias= −1.36, RMSE = 1.67 and R^2= 0.002 site; Figure 10a) and KM83 site (Bias= 0.41, RMSE= 1.50 and R^2= 0.08; Figure 10b) than DTEC GPP. Comparable indices for the DTEC GPP model were: Bias= 0.46, RMSE= 0.75, R^2= 0.43 for the KM67 calibration site (Figure 10a), and Bias= 1.08, RMSE= 1.34, R^2= 0.47 at the KM83 validation site (Figure 10b). We propose that the improvement of the DTEC GPP model over the TL-LUE model arises from linking ε_{msh} for shaded leaves with D_f.

5. Discussion

Regardless of diffuse radiation, big leaf GPP estimates like those of the MOD17 GPP products can simulate the forest GPP seasonality in middle or high latitudes of North America (e.g., the Michigan UMBS site; Table 2 and Figure 3). At the UMBS site, this is mainly due to its seasonal covariation with higher global radiation, diffuse radiation, air temperature, and precipitation in summer (i.e., high sun season) than that in winter (Figure 11). In summary, big leaf GPP models can work well where diffuse radiation and global radiation have seasonal variations that are in phase. In contrast, big leaf GPP models are challenged in ecosystems such as the Amazon rainforest (e.g., KM67 and KM84) where global radiation features opposite phase relations in seasonal variation to diffuse radiation and GPP.

Regardless of differences between sunlit and shaded leaves, some modeling studies have successfully simulated seasonal carbon dynamics in Amazon evergreen forests (Doughty & Goulden, 2008; Kim et al., 2012; Wu et al., 2016). Wu et al. (2016) attributed the seasonal changes of GPP to leaf age composition (i.e., young, mature, and old leaves), their respective photosynthetic capacity (PC; e.g., mature leaves have the highest PC), and LAI. They concluded that aggregate canopy phenology, not climate drivers (i.e., rainfall and PAR), played the dominant role in the seasonality of GPP. However, their studies ignored the potential impact of diffuse radiation as an environmental driver.

Our finding of a significant linear relationship between LUE and D_f reveals a positive response mechanism of forest GPP to atmospheric diffuse radiation in tropical rainforest, which induces the seasonal variation of GPP. This is a factor seldom addressed by previous research. This implies that:

1. Tropical rainforests had acclimatized to their unique environment with higher D_f and diffuse radiation in the wet season and lower D_f in the dry season through biological factors (i.e., LUE and LAI); and
2. Diffuse radiation was the climatic factor dominating seasonal variations of GPP in Amazon rainforests through vegetation phenology (e.g., leaf age composition) and physiological processes (Xia et al., 2015).

Our findings refine previous suggestions that light (i.e., global radiation) is more limiting than water for tropical forest productivity [Nemani et al., 2003), even though some shallow-rooted tropical forest species may suffer from soil drought during dry seasons (Stahl et al., 2013).

The canopy structure parameter, LAI, has been used by two-leaf LUE models as prescribed forcing data to differentiate between sunlit and shaded leaves (He et al., 2013). A key advantage of this approach is that two-leaf LUE models have the capacity to separate photosynthetic contributions of sunlit and shaded leaves to GPP, and to diagnose the impacts of atmospheric radiation changes, such as global dimming or brightening due to changes in aerosol concentration and cloudiness (Wild, 2009), on ecosystem GPP. Because traditional big leaf GPP models and D_f-corrected big leaf GPP models use canopy FPAR as forcing (Chen et al.,

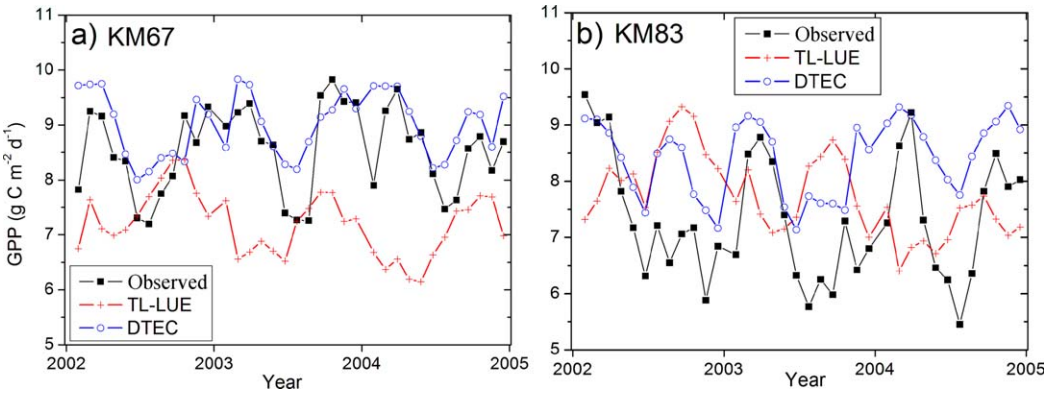

Figure 10. Comparison of monthly estimated TL-LUE GPP and DTEC GPP versus flux tower-observed GPP at KM67 and KM83 Amazon forest sites.

2012), they cannot discern sunlit and shaded leaves. The DTEC model, as a novel remote-sensing LAI-based GPP model, simulated the seasonality of GPP in the Amazon better than alternative models.

Nonetheless, as LAI and FPAR data are often retrieved by different sensors or remote sensing algorithms (Myneni et al., 2002; Zhu et al., 2013), they could contain different errors of estimation and even indicate different climate trends. To evaluate the uncertainty arising from the use of vegetation LAI, we compared DTEC GPP estimates driven with independent LAI dat and FPAR-simply-converted LAI data by using a simple conversion equation (He et al., 2013), respectively. In this comparison, DTEC GPP_{FPAR} driven with MOD15 FPAR-derived LAI (Figure 2c) had error statistics of RMSE= 2.18, Bias= −0.07, and R^2= 0.71 over all sites, similar to that (RMSE= 2.55, Bias= −0.21, and R^2= 0.70) of DTEC GPP driven with MOD15 LAI (Figure 2a). The comparison demonstrates the robustness in the DTEC GPP model.

The DTEC GPP model and the TL-LUE model can be similarly classified as the two-leaf LUE models, however, their parameterization is different, resulting in different performances in the Amazon tropical rainforests.

The TL-LUE model defines both ε_{msh} and ε_{msu} as constant parameters, producing underestimation of GPP and canopy LUE under conditions of high diffuse fraction such as in wet season (He et al., 2013). Based on a biophysical multilayer model, however, Knohl and Baldocchi (2008) pointed out that D_f has little impact on leaf photosynthesis of sunlit leaves while high D_f produces a strong increase in leaf photosynthesis for shaded leaves. Because of its use of ε_{msh} and ε_{msu} dependent on vegetation type (He et al., 2013; Zhou et al., 2016), the TL-LUE model requires a new calibration when extended to new sites.

The DTEC GPP model and the TL-LUE model adopt different definitions of water stress factors. The TL-LUE model simply uses VPD to express the effect of atmospheric water stress while neglecting soil water stress. The DTEC GPP model adopts the ratio of actual E to E_{PT} to include effects of both soil moisture and VPD following the TEC GPP model (Yan et al., 2015). Evaluation shows that E/E_{PT} produces better performance than several other water stress indices, because the VPD-based water stress factor tends to play a bigger role in wet season at sites with ample soil water supply (Yan et al., 2015).

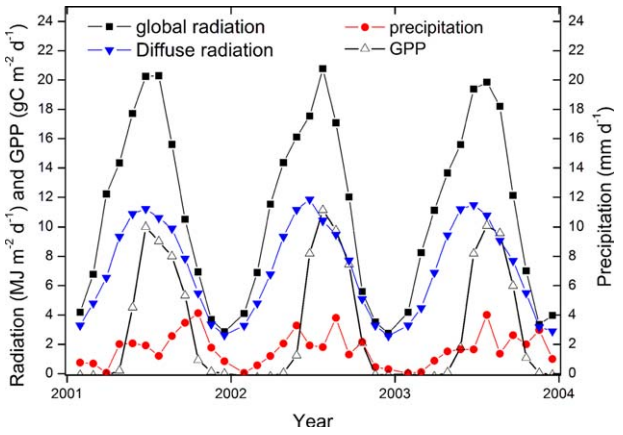

Figure 11. Time series of monthly global radiation, diffuse radiation, precipitation, and GPP at the UMBS site from 2001 to 2003.

It was observed (Alton et al., 2007; de Pury & Farquhar,1997) that sunflecks often produce light saturation at high sky radiance and high temperature under direct sunlight in the afternoon, which results in a lower LUE and a reduced GPP due to stomatal closure on a diurnal scale. But this effect cannot be simulated on daily or monthly scales by remote sensing-based GPP models including the DTEC-GPP model. Normally, sunlit leaves often have higher temperatures than those of shaded leaves, which results in different responses of photosynthesis but is not considered by most big leaf and two-leaf remote sensing GPP models (He et al., 2013). Ignoring temperature differences between sunlit and shaded leaves, however, may not significantly worsen the

accuracy of the DTEC-GPP model because leaf temperature is a second order effect in photosynthesis (Alton et al., 2007).

Significant enhancement of canopy LUE due to diffuse radiation has been reported but is of different magnitudes for crops (110%; *Choudhury*, 2000), broadleaf and needleleaf forests (110%–180%; Gu et al., 2002), a number of boreal needle leaf, temperate broadleaf and tropical broadleaf forests (6%–33%; Alton et al., 2007), tropical savannas (100%; Kanniah et al., 2013), and an Amazon tropical forest (100%; in this study), which demonstrates the sensitivity of canopy LUE to D_f at a site level. On a global scale, global dimming may have enhanced the land carbon sink between 1960 and 1999 due to a 'diffuse-radiation' fertilization effect (Mercado et al., 2009). Clearly, the impact of diffuse radiation should be considered when modeling terrestrial carbon dynamics and associated driving factors (Carrer et al., 2013; Dufrene et al., 2005; Mercado et al., 2009).

To explicitly include clouds or aerosols in the parameterization of D_f, an atmosphere radiation transfer model must to be adopted to simulate their impact on diffuse radiation. This would need additional forcing data such as cloud cover and aerosol optic depth. However, the empirical D_f-based method (He et al., 2013), utilized by the DTEC GPP model, only needs observed-incident global radiation R_g to calculate the diffuse radiation, and the impact of clouds and aerosols on D_f was still considered by the DTEC GPP model. The evaluation of the D_f-based method at five flux tower sites shows its potential in deriving monthly D_f.

6. Conclusions

A novel remote-sensing LAI-based two leaf light use efficiency model (DTEC) is presented. It explicitly considers the impacts of diffuse radiation and water stress on GPP by using a two-leaf GPP modeling structure coupled with a precipitation-driven ARTS *E* model and distinct parameterization for C3 and C4 plants.

With a single calibration at an Amazon rainforest site, the DTEC GPP model was used to simulate photosynthetic seasonality at 20 independent AmeriFlux sites driven with MOD15 LAI data, C3/C4 plant type, flux tower-observed meteorological data, and soil data. One key feature of the DTEC GPP model was that ε_{msh} for shaded leaves was defined as a power function of diffuse fraction D_f and ε_{msu} for sunlit leaves was a constant with their parameterizations only varying between C3 and C4 plant types. This suggests the capacity of being applied to other sites or more species such as forest, crop, and grass without further calibration.

Evaluation at 20 independent flux tower sites showed that DTEC GPP explained the majority (70%) of variability seen in the monthly observed GPP and performed better than MOD17 GPP products, especially for C4 species. Regardless of diffuse radiation, big leaf GPP estimates, such as MOD17 GPP product, might give an seasonal variation opposite in phase to the observed GPP in Amazon forest regions, because big leaf GPP models depend on global radiation which features an opposite seasonal variation in phase to observed GPP in Amazon rainforests.

The DTEC GPP model showed improved performance over the two-leaf TL-LUE GPP model. The DTEC model initially simulated the GPP seasonality in two Amazon forest sites due to linking ε_{msh} for shaded leaves with D_f, while the TL-LUE GPP model could not due to using a constant ε_{msh} for shaded leaves. This result highlights the importance of diffuse radiation and D_f in seasonal GPP simulations, especially in tropical forest ecosystems. The different response of photosynthesis to diffuse and direct radiation should, therefore, be explicitly considered in coupled climate-carbon flux models.

Acknowledgments
We would like to thank the flux site investigators for providing their data through the AmeriFlux program (https://ameriflux.lbl.gov) of the Department of Energy Office of Science, and the Land Processes Distributed Active Archive Center (LP DAAC) for supplying MODIS products (https://lpdaac.usgs.gov/). This work was supported by National Natural Science Foundation of China (41571327, 41171284) and NASA grants to H.H. Shugart: 10-CARBON10–0068, and Climate Change/09-IDS09–116. We also thank the reviewers for their constructive remarks and suggestions.

References

Alton, P. B., North, P. R., & Los, S. O. (2007). The impact of diffuse sunlight on canopy light-use efficiency, gross photosynthetic product and net ecosystem exchange in three forest biomes. *Global Change Biology*, *13*, 776–787. https://doi.org/10.1111/j.1365-2486.2007.01316.x

Baker, I. T., Prihodko, L., Denning, A. S., Goulden, M., Miller, S., & da Rocha, H. R. (2008). Seasonal drought stress in the Amazon: Reconciling models and observations. *Journal of Geophysical Research*, *113*, G00B01. https://doi.org/10.1029/2007JG000644

Baldocchi, D. (1994). A comparative-study of mass and energy-exchange rates over a closed C3 (Wheat) and an open C4 (Corn) crop CO2 exchange and water-use efficiency. *Agricultural and Forest Meteorology*, *67*, 291–321. https://doi.org/10.1016/0168-1923(94)90008-6

Baldocchi, D., Falge, E., Gu, L. H., Olson, R., Hollinger, D., Running, S., . . . Wofsy, S. (2001). FLUXNET: A new tool to study the temporal and spatial variability of ecosystem-scale carbon dioxide, water vapor, and energy flux densities. *Bulletin of the American Meteorological Society*, *82*, 2415–2434. https://doi.org/10.1175/1520-0477(2001)082<2415:FANTTS>2.3.CO;2

Bruno, R. D., da Rocha, H. R., de Freitas, H. C., Goulden, M. L., & Miller, S. D. (2006). Soil moisture dynamics in an eastern Amazonian tropical forest. *Hydrological Processes*, *20*(12), 2477–2489. https://doi.org/10.1002/hyp.6211

Carrer, D., Roujean, J.-L., Lafont, S., Calvet, J.-C., Boone, A., Decharme, B., . . . Gastellu-Etchegorry, J.-P. (2013). A canopy radiative transfer scheme with explicit FAPAR for the interactive vegetation model ISBA-A-gs: Impact on carbon fluxes. *Journal of Geophysical Research: Biogeosciences*, *118*, 888–903. https://doi.org/10.1002/jgrg.20070

Chen, J. M., Liu, J., Cihlar, J., & Goulden, M. L. (1999). Daily canopy photosynthesis model through temporal and spatial scaling for remote sensing applications. *Ecological Modelling*, *124*, 99–119. https://doi.org/10.1016/S0304-3800(99)00156-8

Chen, J. M., Mo, G., Pisek, J., Liu, J., Deng, F., Ishizawa, M., & Chan, D. (2012). Effects of foliage clumping on the estimation of global terrestrial gross primary productivity. *Global Biogeochemical Cycles*, *26*, GB1019. https://doi.org/10.1029/2010GB003996

Cheng, S. J., Bohrer, G., Steiner, A. L., Hollinger, D. Y., Suyker, A., Phillips, R. P., & Nadelhoffer, K. J. (2015). Variations in the influence of diffuse light on gross primary productivity in temperate ecosystems. *Agricultural and Forest Meteorology*, *201*, 98–110. https://doi.org/10.1016/j.agrformet.2014.11.002

Cheng, S. J., Steiner, A. L., Hollinger, D. Y., Bohrer, G., & Nadelhoffer, K. J. (2016). Using satellite-derived optical thickness to assess the influence of clouds on terrestrial carbon uptake. *Journal of Geophysical Research: Biogeosciences*, *121*, 1747–1761. https://doi.org/10.1002/2016jg003365

Choudhury, B. J. (2000). A sensitivity analysis of the radiation use efficiency for gross photosynthesis and net carbon accumulation by wheat. *Agricultural and Forest Meteorology*, *101*, 217–234. https://doi.org/10.1016/S0168-1923(99)00156-2

Coops, N. C., Ferster, C. J., Waring, R. H., & Nightingale, J. (2009). Comparison of three models for predicting gross primary production across and within forested ecoregions in the contiguous United States. *Remote Sensing of Environment*, *113*, 680–690. https://doi.org/10.1016/j.rse.2008.11.013

Cox, P. M., Betts, R. A., Jones, C. D., Spall, S. A., & Totterdell, I. J. (2000). Acceleration of global warming due to carbon-cycle feedbacks in a coupled climate model. *Nature*, *408*, 184–187. https://doi.org/10.1038/35041539

Cramer, W., Bondeau, A., Woodward, F. I., Prentice, I. C., Betts, R. A., Brovkin, V., . . . Young-Molling, C. (2001). Global response of terrestrial ecosystem structure and function to CO2 and climate change: results from six dynamic global vegetation models. *Global Change Biology*, *7*, 357–373. https://doi.org/10.1046/j.1365-2486.2001.00383.x

Cramer, W., Kicklighter, D. W., Bondeau, A., Iii, B. M., Churkina, G., Nemry, B., . . . Intercomparison, T.P.O.F.T.P.N.M. (1999). Comparing global models of terrestrial net primary productivity (NPP): Overview and key results. *Global Change Biology*, *5*, 1–15. https://doi.org/10.1046/j.1365-2486.1999.00009.x

de Pury, D. G. G., & Farquhar, G. D. (1997). Simple scaling of photosynthesis from leaves to canopies without the errors of big-leaf models. *Plant, Cell and Environment*, *20*, 537–557. https://doi.org/10.1111/j.1365-3040.1997.00094.x

Donohue, R. J., Hume, I. H., Roderick, M. L., McVicar, T. R., Beringer, J., Hutley, L. B., . . . Arndt, S. K. (2014). Evaluation of the remote-sensing-based DIFFUSE model for estimating photosynthesis of vegetation. *Remote Sensing of Environment*, *155*, 349–365. https://doi.org/10.1016/j.rse.2014.09.007

Doughty, C. E., & Goulden, M. L. (2008). Seasonal patterns of tropical forest leaf area index and CO2 exchange. *Journal of Geophysical Research*, *113*, G00B06. https://doi.org/10.1029/2007JG000590

Dufrene, E., Davi, H., Francois, C., Maire, G. L., Dantec, V. L., & Granier, A. (2005). Modelling carbon and water cycles in a beech forest: Part I: Model description and uncertainty analysis on modelled NEE. *Ecological Modelling*, *185*, 407–436. https://doi.org/10.1016/j.ecolmodel.2005.01.004

Falge, E., Baldocchi, D., Olson, R., Anthoni, P., Aubinet, M., Bernhofer, C., . . . Wofsy, S. (2001). Gap filling strategies for defensible annual sums of net ecosystem exchange. *Agricultural and Forest Meteorology*, *107*, 43–69. https://doi.org/10.1016/S0168-1923(00)00225-2

Falge, E., Baldocchi, D., Tenhunen, J., Aubinet, M., Bakwin, P., Berbigier, P., . . . Wofsy, S. (2002). Seasonality of ecosystem respiration and gross primary production as derived from FLUXNET measurements. *Agricultural and Forest Meteorology*, *113*, 53–74. https://doi.org/10.1016/S0168-1923(02)00102-8

Farquhar, G. D., & Roderick, M. L. (2003). Pinatubo, diffuse light, and the carbon cycle. *Science*, *299*, 1997–1998. https://doi.org/10.1126/science.1080681

Grant, R. F., Hutyra, L. R., Oliveira, R. C., Munger, J. W., Saleska, S. R., & Wofsy, S. C. (2009). Modeling the carbon balance of Amazonian rain forests: resolving ecological controls on net ecosystem productivity. *Ecological Monographs*, *79*, 445–463. https://doi.org/10.1890/08-0074.1

Gu, L. H., Baldocchi, D., Verma, S. B., Black, T. A., Vesala, T., Falge, E. M., & Dowty, P. R. (2002). Advantages of diffuse radiation for terrestrial ecosystem productivity. *Journal of Geophysical Research*, *107(D6)*, 4050. https://doi.org/10.1029/2001JD001242

Guan, K., Pan, M., Li, H., Wolf, A., Wu, J., Medvigy, D., . . . Lyapustin, A. I. (2015). Photosynthetic seasonality of global tropical forests constrained by hydroclimate. *Nature Geoscience*, *8*, 284–289. https://doi.org/10.1038/ngeo2382

He, M. Z., Ju, W. M., Zhou, Y. L., Chen, J. M., He, H. L., Wang, S. Q., . . . Zhao, F. H. (2013). Development of a two-leaf light use efficiency model for improving the calculation of terrestrial gross primary productivity. *Agricultural and Forest Meteorology*, *173*, 28–39. https://doi.org/10.1016/j.agrformet.2013.01.003

Horn, J. E., & Schulz, K. (2011). Spatial extrapolation of light use efficiency model parameters to predict gross primary production. *Journal of Advances in Modeling Earth Systems*, *3*, M12001. https://doi.org/10.1029/2011MS000070

Houghton, R. A. (2000). Interannual variability in the global carbon cycle. *Journal of Geophysical Research*, *105*, 20121–20130. https://doi.org/10.1029/2000JD900041

Hutyra, L. R., Munger, J. W., Saleska, S. R., Gottlieb, E., Daube, B. C., Dunn, A. L., . . . Wofsy, S. C. (2007). Seasonal controls on the exchange of carbon and water in an Amazonian rain forest. *Journal of Geophysical Research*, *112,* G03008. https://doi.org/10.1029/2006JG000365

Jones, H. G. (1992). *Plants and microclimate: A quantitative approach to environmental plant physiology*. New York, NY: Cambridge University Press.

Kanniah, K. D., Beringer, J., & Hurley, L. (2013). Exploring the link between clouds, radiation, and canopy productivity of tropical savannas. *Agricultural and Forest Meteorology*, *182*, 304–313. https://doi.org/10.1016/j.agrformet.2013.06.010

Kim, Y., Knox, R. G., Longo, M., Medvigy, D., Hutyra, L. R., Pyle, E. H., . . . Moorcroft, P. R. (2012). Seasonal carbon dynamics and water fluxes in an Amazon rainforest. *Global Change Biology*, *18*, 1322–1334. https://doi.org/10.1111/j.1365-2486.2011.02629.x

King, D. A., Turner, D. P., & Ritts, W. D. (2011). Parameterization of a diagnostic carbon cycle model for continental scale application. *Remote Sensing of Environment*, *115*, 1653–1664. https://doi.org/10.1016/j.rse.2011.02.024

Knohl, A., & Baldocchi, D. D. (2008). Effects of diffuse radiation on canopy gas exchange processes in a forest ecosystem. *Journal of Geophysical Research*, *113*, G02023. https://doi.org/10.1029/2007JG000663

Maisongrande, P., Ruimy, A., Dedieu, G., & Saugier, B. (1995). Monitoring seasonal and interannual variations of gross primary productivity, net primary productivity and net ecosystem productivity using a diagnostic model and remotely-sensed data. *Tellus, Series B Chemical and Physical Meteorology*, *47*(1–2), 178–190. https://doi.org/10.1034/j.1600-0889.47.issue1.15.x

Matsui, T., Beltran-Przekurat, A., Niyogi, D., Pielke, R. A., & Coughenour, M. (2008). Aerosol light scattering effect on terrestrial plant productivity and energy fluxes over the eastern United States. *Journal of Geophysical Research*, *113*, D14S14. https://doi.org/10.1029/2007JD009658

McCree, K. J. (1972). Test of current definitions of phtosysthetically active radiation against leaf photosysthesis data. *Agricultural and Forest Meteorology*, *10*, 442–453.

Melillo, J. M., McGuire, A. D., Kicklighter, D. W., Moore, B., Vorosmarty, C. J., & Schloss, A. L. (1993). Global climate change and terrestrial net primary production. *Nature*, *363*(6426), 234–240. https://doi.org/10.1038/363234a0

Mercado, L. M., Bellouin, N., Sitch, S., Boucher, O., Huntingford, C., Wild, M., & Cox, P. M. (2009). Impact of changes in diffuse radiation on the global land carbon sink. *Nature*, *458*, 1014–1017. https://doi.org/10.1038/nature07949

Monteith, J. L. (1972). Solar radiation and productivity in tropical ecosystems. *Journal of Applied Ecology*, *9*, 747–766.

Myneni, R. B., Hoffman, S., Knyazikhin, Y., Privette, J. L., Glassy, J., Tian, Y., . . . Running, S. W. (2002). Global products of vegetation leaf area and fraction absorbed PAR from year one of MODIS data. *Remote Sensing of Environment*, *83*, 214–231. https://doi.org/10.1016/S0034-4257(02)00074-3

Nemani, R., Hashimoto, H., Votava, P., Melton, F., Wang, W., Michaelis, A., . . . White, M. (2009). Monitoring and forecasting ecosystem dynamics using the Terrestrial Observation and Prediction System (TOPS). *Remote Sensing of Environment*, *113*, 1497–1509. https://doi.org/10.1016/j.rse.2008.06.017

Nemani, R. R., Keeling, C. D., Hashimoto, H., Jolly, W. M., Piper, S. C., Tucker, C. J., . . . Running, S. W. (2003). Climate-driven increases in global terrestrial net primary production from 1982 to 1999. *Science*, *300*, 1560–1563. https://doi.org/10.1126/science.1082750

Nepstad, D. C., de Carvalho, C. R., Davidson, E. A., Jipp, P. H., Lefebvre, P. A., Negreiros, G. H., . . . Vieira, S. (1994). The role of deep roots in the hydrological and carbon cycles of Amazonian forests and pastures. *Nature*, *372*, 666–669.

Norman, J. M. (1982). Simulation of microclimates. In J. L. Hatfield & I. J. Thomason (Eds.), *Biometeorology in integrated pest management* (pp. 65–99). New York: Academic Press.

Potter, C. S., Randerson, J. T., Field, C. B., Matson, P. A., Vitousek, P. M., Mooney, H. A., & Klooster, S. A. (1993). Terrestrial ecosystem production––A process model-based on global satellite and surface data. *Global Biogeochemical Cycles*, *7*, 811–841.

Priestley, C. H., & Taylor, R. J. (1972). Assessment of surface heat-flux and evaporation using large-scale parameters. *Monthly Weather Review*, *100*, 81–92.

Prince, S. D., & Goward, S. N. (1995). Global primary production: A remote sensing approach. *Journal of Biogeography*, *22*, 815–835.

Raich, J. W., Rastetter, E. B., Melillo, J. M., Kicklighter, D. W., Steudler, P. A., Peterson, B. J., . . . Vorosmarty, C. J. (1991). Potential net primary productivity in South-America––Application of a global model. *Ecological Applications*, *1*, 399–429.

Roderick, M. L., Farquhar, G. D., Berry, S. L., & Noble, I. R. (2001). On the direct effect of clouds and atmospheric particles on the productivity and structure of vegetation. *Oecologia*, *129*, 21–30. https://doi.org/10.1007/s004420100760

Running, S. W., Nemani, R. R., Heinsch, F. A., Zhao, M. S., Reeves, M., & Hashimoto, H. (2004). A continuous satellite-derived measure of global terrestrial primary production. *BioScience*, *54*, 547–560. https://doi.org/10.1641/0006-3568(2004)054[0547:ACSMOG]2.0.CO;2

Running, S. W., Thornton, P. E., Nemani, R., & Glassy, J. M. (2000). Global terrestrial gross and net primary productivity from the Earth Observing System. In O. E. Sala, R. B. Jackson, H. A. Mooney, & R. W. Howarth (Eds.), *Methods in ecosystem science*. (pp. xxii, 421 p., 423 p. of plates). New York, NY: Springer.

Saxton, K. E., Rawls, W. J., Romberger, J. S., & Papendick, R. I. (1986). Estimating generalized soil-water characteristics from texture. *Soil Science Society of America Journal*, *50*, 1031–1036.

Sellers, P. J., Berry, J. A., Collatz, G. J., Field, C. B., & Hall, F. G. (1992). Canopy reflectance, photosynthesis, and transpiration. III. A reanalysis using improved leaf models and a new canopy integration scheme. *Remote Sensing of Environment*, *42*, 187–216. https://doi.org/10.1016/0034-4257(92)90102-P

Stahl, C., Burban, B., Wagner, F., Goret, J.-Y., Bompy, F., & Bonal, D. (2013). Influence of seasonal variations in soil water availability on gas exchange of tropical canopy trees. *Biotropica*, *45*(2), 155–164. https://doi.org/10.1111/j.1744-7429.2012.00902.x

Turner, D. P., Ritts, W. D., Styles, J. M., Yang, Z., Cohen, W. B., Law, B. E., & Thornton, P. E. (2006). A diagnostic carbon flux model to monitor the effects of disturbance and interannual variation in climate on regional NEP. *Tellus, Series B––Chemical and Physical Meteorology*, *58*, 476–490. https://doi.org/10.1111/j.1600-0889.2006.00221.x

Verbeeck, H., Peylin, P., Bacour, C., Bonal, D., Steppe, K., & Ciais, P. (2011). Seasonal patterns of CO2 fluxes in Amazon forests: Fusion of eddy covariance data and the ORCHIDEE model. *Journal of Geophysical Research*, *116*, G02018. https://doi.org/10.1029/2010JG001544

Verma, S. B., Dobermann, A., Cassman, K. G., Walters, D. T., Knops, J. M., Arkebauer, T. J., . . . Walter-Shea, E. A. (2005). Annual carbon dioxide exchange in irrigated and rainfed maize-based agroecosystems. *Agricultural and Forest Meteorology*, *131*, 77–96. https://doi.org/10.1016/j.agrformet.2005.05.003

Wang, B., Shugart, H. H., Shuman, J. K., & Lerdau, M. T. (2016). Forests and ozone: productivity, carbon storage, and feedbacks. *Scientific Reports*, *6*, 22133. https://doi.org/10.1038/Srep22133

Wang, S., Huang, K., Yan, H., Yan, H., Zhou, L., Wang, H., . . . Sun, L. (2015). Improving the light use efficiency model for simulating terrestrial vegetation gross primary production by the inclusion of diffuse radiation across ecosystems in China. *Ecological Complexity*, *23*, 1–13. https://doi.org/10.1016/j.ecocom.2015.04.004

Waring, R. H., Law, B. E., Goulden, M. L., Bassow, S. L., McCreight, R. W., Wofsy, S. C., & Bazzaz, F. A. (1995). Scaling gross ecosystem production at Harvard Forest with remote sensing: a comparison of estimates from a constrained quantum-use efficiency model and eddy correlation. *Plant, Cell & Environment*, *18*, 1201–1213. https://doi.org/10.1111/j.1365-3040.1995.tb00629.x

Wild, M. (2009). Global dimming and brightening: A review. *Journal of Geophysical Research*, *114*, D00D16. https://doi.org/10.1029/2008JD011470

Wu, J., Albert, L. P., Lopes, A. P., Restrepo-Coupe, N., Hayek, M., Wiedemann, K. T., . . . Saleska, S. R. (2016). Leaf development and demography explain photosynthetic seasonality in Amazon evergreen forests. *Science*, *351*, 972–976. https://doi.org/10.1126/science.aad5068

Xia, J. Y., Niu, S. L., Ciais, P., Janssens, I. A., Chen, J. Q., Ammann, C., . . . Luo, Y. Q. (2015). Joint control of terrestrial gross primary productivity by plant phenology and physiology. *Proceedings of the National Academy of Sciences of the United States of America*, *112*, 2788–2793. https://doi.org/10.1073/pnas.1413090112

Xiao, X. M., Zhang, Q. Y., Braswell, B., Urbanski, S., Boles, S., Wofsy, S., . . . Ojima, D. (2004). Modeling gross primary production of temperate deciduous broadleaf forest using satellite images and climate data. *Remote Sensing of Environment*, *91*, 256–270. https://doi.org/10.1016/j.rse.2004.03.010

Yan, H., Wang, S. Q., Billesbach, D., Oechel, W., Bohrer, G., Meyers, T., . . . Shugart, H. H. (2015). Improved global simulations of gross primary product based on a new definition of water stress factor and a separate treatment of C3 and C4 plants. *Ecological Modelling*, *297*, 42–59. https://doi.org/10.1016/j.ecolmodel.2014.11.002

Yan, H., Wang, S. Q., Billesbach, D., Oechel, W., Zhang, J. H., Meyers, T., . . . Scott, R. (2012). Global estimation of evapotranspiration using a leaf area index-based surface energy and water balance model. *Remote Sensing of Environment*, *124*, 581–595. https://doi.org/10.1016/j.rse.2012.06.004

Yan, H., Yu, Q., Zhu, Z.-C., Myneni, R. B., Yan, H.-M., Wang, S.-Q., Shugart, H. H. (2013). Diagnostic analysis of interannual variation of global land evapotranspiration over 1982–2011: Assessing the impact of ENSO. *Journal of Geophysical Research: Atmospheres*, *118*, 8969–8983. https://doi.org/10.1002/jgrd.50693

Yan, H., Wang, S.-Q., Lu, H.-Q., Yu, Q., Zhu, Z.-C., Myneni, R. B., Liu, Q., & Shugart, H. H. (2014). Development of a remotely sensing seasonal vegetation-based Palmer Drought Severity Index and its application of global drought monitoring over 1982–2011. *Journal of Geophysical Research: Atmospheres*, *119*, 9419–9440. https://doi.org/10.1002/2014JD021673

Yang, W. Z., Huang, D., Tan, B., Stroeve, J. C., Shabanov, N. V., Knyazikhin, Y., . . . Myneni, R. B. (2006). Analysis of leaf area index and fraction of PAR absorbed by vegetation products from the terra MODIS sensor: 2000–2005. *IEEE Transactions on Geoscience and Remote Sensing*, *44*, 1829–1842. https://doi.org/10.1109/Tgrs.2006.871214

Zhang, F., Chen, J. M., Chen, J., Gough, C. M., Martin, T. A., & Dragoni, D. (2012). Evaluating spatial and temporal patterns of MODIS GPP over the conterminous U.S. against flux measurements and a process model. *Remote Sensing of Environment*, *124*, 717–729. https://doi.org/10.1016/j.rse.2012.06.023

Zhao, M. S., Heinsch, F. A., Nemani, R. R., & Running, S. W. (2005). Improvements of the MODIS terrestrial gross and net primary production global data set. *Remote Sensing of Environment*, *95*, 164–176. https://doi.org/10.1016/j.rse.2004.12.011

Zhou, Y., Wu, X., Ju, W., Chen, J. M., Wang, S., Wang, H., . . . Varlagin, A. (2016). Global parameterization and validation of a two-leaf light use efficiency model for predicting gross primary production across FLUXNET sites. *Journal of Geophysical Research: Biogeosciences*, *121*, 1045–1072. https://doi.org/10.1002/2014JG002876

Zhu, Z. C., Bi, J., Pan, Y. Z., Ganguly, S., Anav, A., Xu, L., . . . Myneni, R. B. (2013). Global Data Sets of Vegetation Leaf Area Index (LAI)3g and Fraction of Photosynthetically Active Radiation (FPAR)3g Derived from Global Inventory Modeling and Mapping Studies (GIMMS) Normalized Difference Vegetation Index (NDVI3g) for the Period 1981 to 2011. *Remote Sensing*, *5*, 927–948. https://doi.org/10.3390/rs5020927